

Fluctuating superconductivity in overdoped cuprate with a flat antinodal dispersion

Yu He^{*,1,2,3,4} Su-Di Chen^{*,1,3} Zi-Xiang Li^{*,2} Dan Zhao^{5,6} Dongjoon Song⁷ Yoshiyuki Yoshida,⁷ Hiroshi Eisaki,⁷ Tao Wu,^{5,6} Xian-Hui Chen,^{5,6} Dong-Hui Lu,⁸ Christoph Meingast,⁹ Robert J. Birgeneau,^{2,4} Thomas P. Devereaux,^{10,3} Makoto Hashimoto^{†,8} Dung-Hai Lee^{†,2,4} and Zhi-Xun Shen^{†1,3}

¹*Department of Applied Physics, Stanford University, Stanford, CA 94305, USA*

²*Department of Physics, University of California at Berkeley, Berkeley, CA 94720, USA*

³*Stanford Institute for Materials and Energy Sciences,*

SLAC National Accelerator Laboratory, 2575 Sand Hill Road, Menlo Park, CA 94025, USA

⁴*Materials Sciences Division, Lawrence Berkeley National Laboratory, Berkeley, CA 94720, USA**

⁵*Hefei National Laboratory for Physical Sciences at the Microscale,*

University of Science and Technology of China, Hefei, Anhui 230026, China

⁶*CAS Key Laboratory of Strongly-coupled Quantum Matter Physics, Department of Physics,*

University of Science and Technology of China, Hefei, Anhui 230026, China

⁷*National Institute of Advanced Industrial Science and Technology, Tsukuba 305-8565, Japan*

⁸*Stanford Synchrotron Radiation Lightsource, SLAC National Accelerator Laboratory, Menlo Park, CA 94025, USA*

⁹*Institute for Quantum Materials and Technologies,*

Karlsruhe Institute of Technology, 76021 Karlsruhe, Germany

¹⁰*Department of Materials Science and Engineering, Stanford University, Stanford, CA 94305, USA*

A major unsolved puzzle in cuprate superconductivity is that, despite accumulated evidence of more conventional normal state properties over the last 30 years, the superconducting T_c of the overdoped cuprates seems to be still controlled by phase coherence¹⁻³ rather than the Cooper pair formation. So far, a microscopic understanding of this unexpected behavior is lacking. Here we report angle-resolved photoemission, magnetic and thermodynamic evidence that Cooper pairs form at temperatures more than 30% above T_c in overdoped metallic $\text{Bi}_2\text{Sr}_2\text{CaCu}_2\text{O}_{8+\delta}$ (Bi-2212). More importantly, our data lead to a microscopic understanding where the phase fluctuation is enhanced by the flat dispersion near the Brillouin zone boundary. This proposal is tested by a sign-problem free quantum Monte Carlo simulation. Such a microscopic mechanism is likely to find applications in other flat band superconductors, such as twisted bilayer-bilayer graphene⁴ and NdNiO_2 ^{5,6}.

In conventional superconductors the superconducting (SC) transition temperature (T_c) is controlled by the formation of Cooper pairs (the BCS paradigm). However, this is shown to be violated in the underdoped (UD) to optimally doped (OP) cuprate^{1,7-9}. There, it is the condensation of Cooper pairs - establishment of phase coherence - that determines T_c . Moreover, the normal states of UD and OP cuprates exhibit pseudogap and strange metal behaviors, making it unclear how Cooper pairs are formed. In contrast, in overdoped (OD) cuprates, transport^{10,11}, thermodynamic¹² and single particle probes¹³⁻¹⁶ all point to a more conventional metallic normal state. This leads to widely held belief that the BCS paradigm has a chance to succeed here. Therefore, it is quite a surprise when recent measurements show that it is also phase coherence that determines T_c in overdoped $(\text{La,Sr})_2\text{CuO}_4$ (LSCO)^{2,3,17}. This puzzle, namely what suppresses the superfluid density and phase stiffness in overdoped cuprates, is what we set out to address.

Overdoped bilayer cuprate $(\text{Pb,Bi})_2\text{Sr}_2\text{CaCu}_2\text{O}_{8+\delta}$ (Pb:Bi-2212) is chosen for its excellent cleavability and large superconducting energy scale. Pressurized oxygen annealing is used to reach $66\text{ K} > T_c > 51\text{ K}$, which corresponds to nominal hole doping of $0.22 < p < 0.24$ ¹⁸. Figure 1 shows the magnetic and thermodynamic signatures of a superconducting transition at $T_c = 66\text{ K}$ ($p = 0.22$). A sharp superconducting transition defined by the

Meissner diamagnetism (Fig. 1(a)) coincides to within 1 K with the zero-resistivity temperature (Fig. 1(b)) and the weak singularity in both the in-plane lattice expansivity (Fig. 1(c)) and heat capacity (Fig. 1(d)). These results are consistent with a sharp, yet non-mean-field phase transition.

To obtain a microscopic understanding, we investigate near the SC gap opening temperature (T_{gap}) and the zero-resistivity temperature (T_c) using high resolution angle-resolved photoemission spectroscopy (ARPES) and ⁶³Cu nuclear magnetic resonance (NMR). Systematic high resolution ARPES in this temperature and doping regime is made possible by the recent advance in localized heating method^{15,19} (see also SI).

First, well-defined single particle spectral peaks are found over the untruncated normal state Fermi surface well above T_c (Fig. 2(a)(j), SI), indicating a more metallic normal state compared to OP samples¹⁵. Experimentally fitted Fermi surface volumes yield an averaged doping of $p = 0.26$ between the bonding and antibonding sheets ($p_{\text{AB}} = 0.34$, $p_{\text{BB}} = 0.18$), slightly larger than the doping deduced from the empirical parabolic T_c - p relation^{18,37}. A d -wave gap is observed to uniformly close over the entire momentum space upon warming (SI). To determine T_{gap} , high statistics energy-momentum cut along the Brillouin zone (BZ) boundary (red line in Fig. 2(a)) is measured between 10 K and 150 K (Fig. 2(b)-(j)) with an energy resolution of 8 meV. The Fermi function is di-

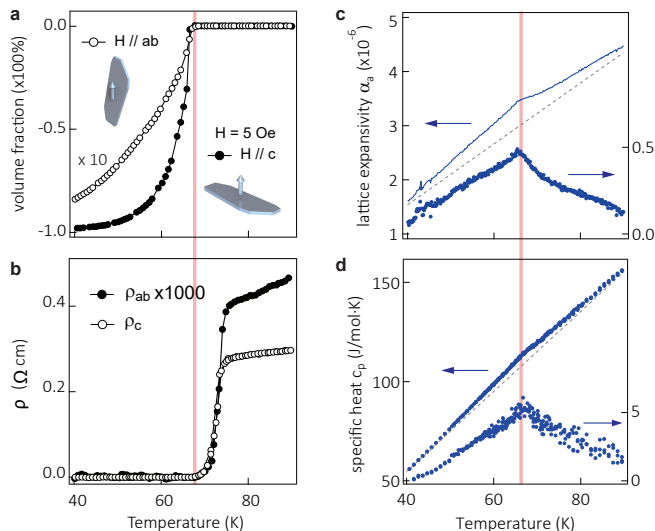


FIG. 1: Bulk magnetic and thermodynamic properties of a heavily overdoped Bi-2212 with $T_c = 66$ K. (a) DC diamagnetic response at 5 Oe, for fields both perpendicular (solid) and parallel (open) to the CuO_2 -plane. (b) In- and out-of-plane resistivity near T_c . (c) In-plane linear lattice expansion coefficient α . (d) Molar specific heat c_p . In both (c) and (d), a linear background (grey dash) is removed to highlight the superconducting transition in the bottom curve plotted to the right axes on an enlarged scale.

vided from the spectra to reveal the unoccupied states (for detailed procedures and raw EDCs see SI). Enabled by excellent statistics and resolution, both the electron and hole branches of the Bogoliubov quasiparticle dispersions can be traced out around T_c (Fig. 2(k)). The superconducting gap decreases from 10 K up to 63 K, yet a sizeable spectral gap remains at T_c (Fig. 2(k), cyan markers). In fact, above T_c it continues to close and fill up until it becomes indiscernible around 86 K. During this process, the particle-hole symmetry - evidenced by the dispersion (Fig. 2(k)) and intensity (Fig. 2(l)) of electron and hole branches of the Bogoliubov quasiparticles - remains preserved down to 1.5 meV uncertainty (grey band in Fig. 2(k)), which is accountable by the finite resolution effect (see SI). This particle-hole symmetric normal state gap suggests the presence of Cooper pairing beyond the nodal region¹⁹, and is fundamentally different from the incoherent, particle-hole asymmetric pseudogap in the UD and OP cuprates (see SI)^{15,20}.

To quantify the particle-hole mixing near the antinodal region, Fig. 2(l) shows the Bogoliubov angle²¹ $\theta_{\mathbf{k}} = \tan^{-1} |v_{\mathbf{k}}/u_{\mathbf{k}}|$ for temperatures near T_c . Here, $u_{\mathbf{k}}^2$ ($v_{\mathbf{k}}^2$) are the quasiparticle spectral intensities below and above the Fermi energy. Accordingly, $\theta_{\mathbf{k}} = 0, \pi/2$ and $\pi/4$ indicate pure electron (particle), pure hole, and equal particle-hole mixture respectively. For conventional superconductors $\theta_{\mathbf{k}}$ only deviates from 0 or $\pi/2$ in the vicinity

of Fermi momenta \mathbf{k}_F . However in overdoped Bi-2212 $\theta_{\mathbf{k}}$ is centered around $\pi/4$ for the entire Bogoliubov quasiparticle band around the antinode. We attribute this to the flatness of the normal state antinodal dispersion in comparison to the size of the superconducting gap.³⁸

The electronic structure undergoes three distinct stages of evolution as a function of temperature. Figure 3(a)(b) track the temperature dependence of the energy distribution curve (EDC) at the antinodal \mathbf{k}_F and $(\pi,0)$ on the antibonding band. **(1)** Cooling towards ~ 90 K (green lines), the spectral peak gradually sharpens in width and grows in height (for the full temperature range up to 290 K, see SI). **(2)** An energy gap gradually opens below T_{gap} . It starts as the zero-energy spectral intensity saturates, which then further splits into two largely overlapping peaks at T_c (red lines). **(3)** Further cooling from T_c instigates a rapid sharpening of the Bogoliubov quasiparticle peak, as well as a concomitant rapid depletion of the zero-energy spectral weight until a near-complete energy gap forms. Figure 3(c)(d)(i) quantitatively describe in the temperature evolution of the superconducting gap size, spectral peak height, and linewidth (fitted by a Gaussian between -20 meV and 1 meV) at the antinodal \mathbf{k}_F and $(\pi,0)$. In particular, taking advantage of the shallow van Hove point, the superconducting gap at $(\pi,0)$ may be extracted with excellent numerical stability via subtraction of quadrature $\Delta_{\mathbf{k}} = \sqrt{E_{\mathbf{k}}^2 - \epsilon_{\mathbf{k}}^2}$ (Fig. 3(c), blue circles; see also SI). $E_{\mathbf{k}}$ and $\epsilon_{\mathbf{k}}$ are superconducting state and normal state dispersions.

While the momentum resolved single particle spectra most clearly show both T_{gap} and T_c , the onset of zero-energy spectral weight depletion also signifies T_{gap} (Fig. 3(e)). This is true both near the antinode shown by ARPES (blue and yellow circles), and as a momentum average shown by the Knight shift of ^{63}Cu nuclear magnetic resonance (red circles). Consistent ARPES and NMR signatures are also observed in 23% and 24% hole-doped Bi-2212 (see SI). The fact that bulk probes, such as NMR, yield results consistent with the surface sensitive ARPES results further supports that the observed fluctuation is a bulk phenomenon. The spectral features shown in Fig. 3(a)-(e) can be excellently reproduced in a spectral simulation with only two inputs (Fig. 3(f)-(h)): a BCS-type $\Delta(T)$ with a 16 meV zero-temperature BCS gap opening at $T_{\text{gap}} \sim 87$ K (Fig. 3(f) black line), and a temperature-dependent linewidth (Fig. 3(i) black line) approximated from experimental measurements (Fig. 3(i) blue circles, see supplement for details). It is worth noting that spectral features around T_c are caused by the sudden reduction of spectral linewidth instead of the gap opening. To sum up, there's a clear mismatch between the bulk gap-opening temperature $T_{\text{gap}} \sim 90$ K and the bulk superconducting transition temperature $T_c = 66$ K. Moreover, the relation between T_{gap} and the zero temperature gap Δ_0 agrees excellently with $\frac{2\Delta_0}{k_B T_{\text{gap}}} \sim 4.3$, the value expected for the d -wave BCS theory.²²

Our data points to a rather conventional gap opening intervened by strong phase fluctuations before coherence

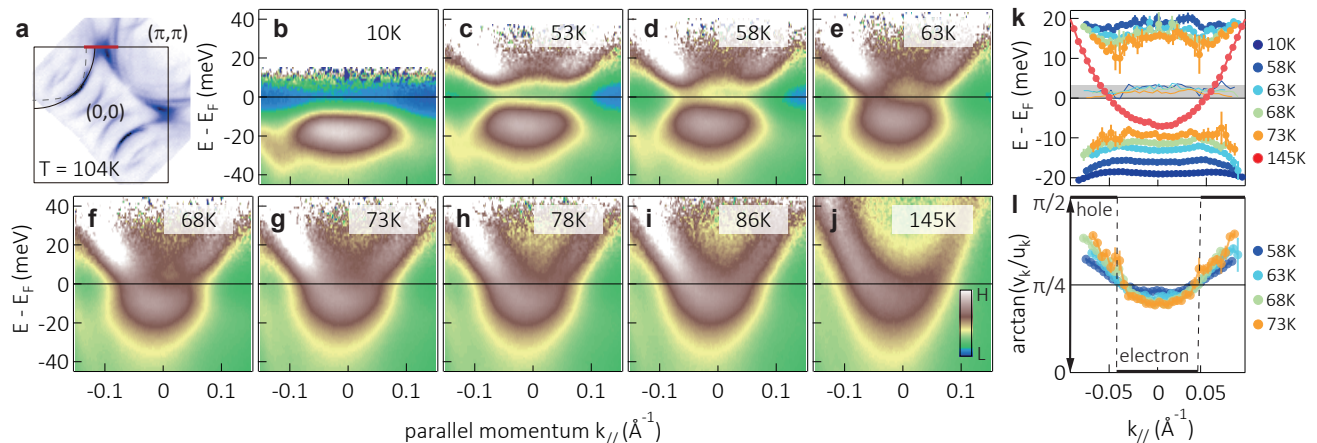


FIG. 2: Temperature dependent high resolution antinodal energy-momentum spectra in heavily overdoped Bi-2212 with $T_c = 66$ K. (a) Fermi surface map integrated within 10 meV of the chemical potential of a Pb-free sample in the normal state. Red bar denotes the parallel momentum of the spectra shown in subsequent panels. (b)-(j) Fermi-function-divided antinodal spectra along the BZ boundary in a Pb-doped sample. (k) Fitted energy-momentum dispersions of both the electron and hole Bogoliubov quasiparticles at various temperatures. Red circles indicate the normal state dispersion at 145 K. Thin lines shaded in grey are the averaged energies of the electron and hole Bogoliubov quasiparticle branches. (l) Calculated particle-hole mixing ratio, expressed in its arc tangent value, from the fitted intensity ratio of the electron and hole Bogoliubov quasiparticle branches near T_c . $\pi/4$ represents equal particle-hole mixture. Black line shows the BCS expectation when $\mathbf{v}_F \cdot \mathbf{k}_F \gg \Delta$.

is achieved. This is consistent with the surprising observation of low zero temperature superfluid density in overdoped LSCO³. However, the microscopic mechanism underlying the low superfluid density is so far lacking. Disorder is an obvious candidate. But for Bi2212 in the doping range we studied, strong disorder seems to be at odds with the continuously sharpening superconducting quasiparticle peak, increasing normal state conductivity, and decreasing in-plane/out of plane resistive anisotropy with doping^{23,24}. Here we point out a hitherto overlooked factor which contributes to the superfluid density reduction, namely, the flat dispersion near the antinode. To test the viability of this proposal, we study a model system with a similar flat dispersion in the absence of disorder.

It is well known that a flat band comes with a large effective mass, hence low superfluid density. However, for overdoped cuprates, the band dispersion is only flat near the antinode. This raises the interesting question of *what the effect on superfluid density will be if flat band dispersion only exists in part of the Brillouin zone*. We address this question with a sign-problem free quantum Monte-Carlo simulation on similar band structure as overdoped cuprates.

To get rid of the fermion sign problem, and still maintain the strongest pairing interaction at the antinode, we choose a model where the band structure is tuned to mimic that of overdoped cuprate, while the pairing interaction is mediated by a d -form factor (B_{1g}) Einstein phonon coupled at $\lambda = 0.25$.³⁹ We compare the quantum Monte Carlo results for band structures without and with a flat antinodal dispersion. The chosen dispersions

(near $(\pi, 0)$) are shown in Fig. 4(a)(b) (experimental band structure is shown in Fig. 4(c)). In both cases, the system exhibits highly anisotropic s -wave superconducting ground state with the gap maximum at $(\pi, 0)$.

Figure 4(d) and (e) plot temperature dependent EDCs near the antinode for band structures shown in (a) and (b) respectively.⁴⁰ The superconducting gap opening temperature T_{gap} , identified by the closure of the antinodal spectral gap, is 33% higher in the case where the band structure is flat at in the antinodal region. This is because the pairing interaction mediated by the B_{1g} phonon can take advantage of the large density of states where flat band exists. On the other hand, the Kosterlitz-Thouless T_c for band structure with a flat antinodal dispersion is only 3% higher (see SI for T_c determination), leaving a much wider temperature window where the gap has opened but phase coherence has yet to establish. Consistent with the enhanced thermal fluctuations above T_c , the zero temperature superfluid density - the quantity central to previous magnetic and optical investigations^{3,17} - is 45% lower with the flat dispersion with quantum fluctuations considered²⁵. These results suggest that even without disorder, the flat dispersion near the antinode plays an important role in suppressing the superfluid density (or the normal state Drude weight) in clean systems.

Real systems always contain disorder, which is also expected to suppress the superfluid density. In this regard, the flat band dispersion amplifies the effect of disorder via increased scattering between antinodes, which is pair breaking due to the d -wave symmetry²⁶. Hence the flat dispersion and disorder can have a combined role in driv-

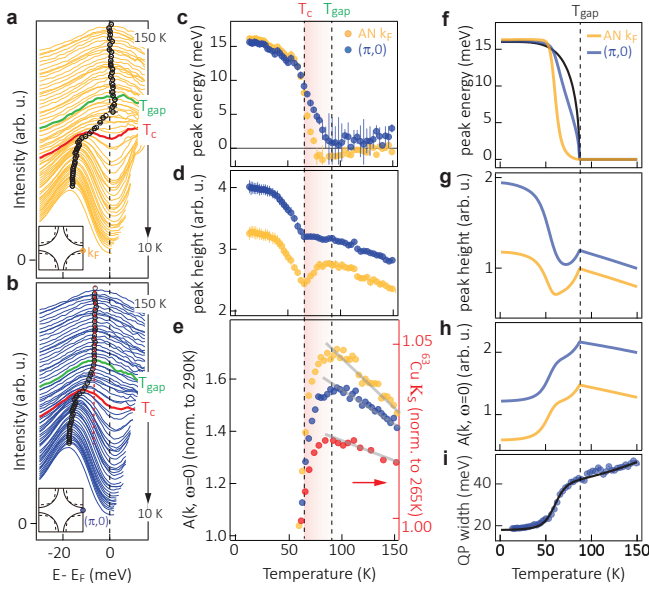


FIG. 3: Temperature dependence of the antinodal EDCs. Fermi-function divided EDCs at (a) antinodal \mathbf{k}_F and (b) $(\pi,0)$. Insets depicts the two momenta in the Brillouin zone. Spectra are normalized to 1 over $[0,100]$ meV binding energy. Green and red lines denote $T_{\text{gap}} \sim 90$ K and $T_c \sim 66$ K respectively. Black circles mark the apparent spectral peak position, and the red-dashed line marks the ungapped van Hove point position. Temperature dependent (c) spectral peak binding energy, (d) spectral peak height, and (e) spectral intensity at E_F from the antinodal \mathbf{k}_F (yellow) and $(\pi,0)$ (blue). Right axis in (e) corresponds to the frequency shift from the ^{63}Cu nuclear spin resonance (red). Grey lines are guides to exemplify normal state spectral weight evolution. (f) Spectral peak binding energy, (g) spectral peak height, and (h) spectral intensity at E_F extracted from the simulated spectra at the antinodal \mathbf{k}_F (yellow) and $(\pi,0)$ (blue), using the same analysis as (c)-(e). Black line in (f) is the BCS gap used for simulation, set to open at 87 K. The vertical shades in (c)-(e) indicate the superconducting fluctuation region. (i) Spectral peak linewidth fitted from $(\pi,0)$ (blue), and the linewidth used for simulation (black). Curves in (d)(g)(h) are offset for clarity.

ing the superconductor to metal transition in the heavily hole-doped cuprates. The answer to which effect is dominant will likely depend on families of compounds. Moreover, the cooperative effects of flat band and disorder is likely to play a role in the strong fluctuations suggested in twisted bilayer-bilayer graphene⁴ and nickelates^{5,27}. In practice, our results provide not only clear band structure targets to engineer the phase stiffness, but also the basis for T_c enhancement at the interface between superconductors with strong pairing and those with large phase stiffness²⁸.

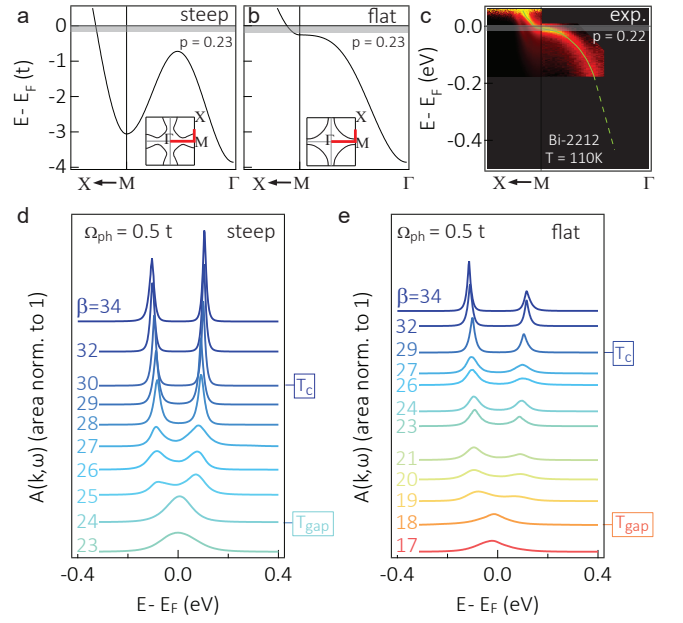


FIG. 4: Band structure contribution to the superconducting fluctuation examined by quantum Monte Carlo simulations. Tight-binding band structures with (a) a steep dispersion and (b) a shallow and flat dispersion near $(\pi,0)$. The along high symmetry cuts are shown by red lines on their respective Fermi surfaces in the insets. (c) Experimentally measured normal state spectra along the same high symmetry cuts for $p = 0.22$ samples. Grey bars are the superconducting gap sizes. Calculated temperature dependent single particle spectra at the antinode for (d) the steep dispersion and (e) the shallow flat dispersion, when anisotropic superconductivity is induced by a B_{1g} phonon. Spectral intensity is normalized so the total area is 1. The curves are offset proportional to temperature $T = 1/\beta$. The electron-phonon coupling strength λ is set to 0.25.

Acknowledgement

The authors wish to thank Steve Kivelson, Edwin Huang, Yao Wang, Junfeng He, Douglas Scalapino, Yoni Schattner, Jiecheng Zhang, Erik Kountz, Jörg Schmalian and Jan Zaanen for helpful discussions. The works at Stanford University and Stanford Synchrotron Radiation Lightsource, SLAC National Accelerator Laboratory, are supported by the U.S. Department of Energy, Office of Science, Office of Basic Energy Sciences under Contract No. DE-AC02-76SF00515. Part of this work is performed at the Stanford Nano Shared Facilities (SNSF), supported by the National Science Foundation under award ECCS-1542152. The works at University of California, Berkeley are supported by U.S. Department of Energy, Office of Science, Office of Basic Energy Sciences, Materials Sciences and Engineering Division under Contract No. DE-AC02-05-CH11231 within the Quantum Materials Program (KC2202). The computational part of this

research is supported by the U.S. Department of Energy, Office of Science, Office of Advanced Scientific Computing Research, Scientific Discovery through Advanced Computing (SciDAC) program. TW and XHC acknowledge the support from the National Key R&D Program of the MOST (Grant No. 2017YFA0303001) and the Na-

tional Natural Science Foundation of China (Grants No. 11888101). DHL acknowledges support from the Gordon and Betty Moore Foundation's EPiQS initiative Grant GBMF4545. YH acknowledges support from the Miller Institute for Basic Research in Science.

-
- * These authors contributed equally to this work.
- ¹ Y. Uemura, G. Luke, B. Sternlieb, J. Brewer, J. Carolan, W. Hardy, R. Kadono, J. Kempton, R. Kiefl, S. Kretitzman, *et al.*, *Physical Review Letters* **62**, 2317 (1989).
 - ² P. M. Rourke, I. Mouzopoulou, X. Xu, C. Panagopoulos, Y. Wang, B. Vignolle, C. Proust, E. V. Kurganova, U. Zeitler, Y. Tanabe, *et al.*, *Nature Physics* **7**, 455 (2011).
 - ³ I. Božović, X. He, J. Wu, and A. Bollinger, *Nature* **536**, 309 (2016).
 - ⁴ X. Liu, Z. Hao, E. Khalaf, J. Y. Lee, Y. Ronen, H. Yoo, D. H. Najafabadi, K. Watanabe, T. Taniguchi, A. Vishwanath, *et al.*, *Nature* **583**, 221 (2020).
 - ⁵ D. Li, K. Lee, B. Y. Wang, M. Osada, S. Crossley, H. R. Lee, Y. Cui, Y. Hikita, and H. Y. Hwang, *Nature* **572**, 624 (2019).
 - ⁶ D. Cho, K. Bastiaans, D. Chatzopoulos, G. Gu, and M. Allan, *Nature* **571**, 541 (2019).
 - ⁷ J. Corson, R. Mallozzi, J. Orenstein, J. N. Eckstein, and I. Bozovic, *Nature* **398**, 221 (1999).
 - ⁸ A. T. Bollinger, G. Dubuis, J. Yoon, D. Pavuna, J. Misewich, and I. Božović, *Nature* **472**, 458 (2011).
 - ⁹ V. Emery and S. Kivelson, *Nature* **374**, 434 (1995).
 - ¹⁰ Y. Ando, S. Komiya, K. Segawa, S. Ono, and Y. Kurita, *Physical Review Letters* **93**, 267001 (2004).
 - ¹¹ C. Proust, E. Boaknin, R. Hill, L. Taillefer, and A. Mackenzie, *Physical Review Letters* **89**, 147003 (2002).
 - ¹² J. Tallon, J. Storey, and J. Loram, *Physical Review B* **83**, 092502 (2011).
 - ¹³ Z. Yusof, B. Wells, T. Valla, A. Fedorov, P. Johnson, Q. Li, C. Kendziora, S. Jian, and D. Hinks, *Physical Review Letters* **88**, 167006 (2002).
 - ¹⁴ Y.-D. Chuang, A. Gromko, A. Fedorov, Y. Aiura, K. Oka, Y. Ando, M. Lindroos, R. Markiewicz, A. Bansil, and D. Dessau, *Physical Review B* **69**, 094515 (2004).
 - ¹⁵ S.-D. Chen, M. Hashimoto, Y. He, D. Song, K.-J. Xu, J.-F. He, T. P. Devereaux, H. Eisaki, D.-H. Lu, J. Zaanen, *et al.*, *Science* **366**, 1099 (2019).
 - ¹⁶ K. Fujita, C. K. Kim, I. Lee, J. Lee, M. Hamidian, I. Fermo, S. Mukhopadhyay, H. Eisaki, S. Uchida, M. Lawler, *et al.*, *Science* **344**, 612 (2014).
 - ¹⁷ F. Mahmood, X. He, I. Božović, and N. Armitage, *Physical Review Letters* **122**, 027003 (2019).
 - ¹⁸ M. Presland, J. Tallon, R. Buckley, R. Liu, and N. Flower, *Physica C: Superconductivity* **176**, 95 (1991).
 - ¹⁹ T. Kondo, W. Malaeb, Y. Ishida, T. Sasagawa, H. Sakamoto, T. Takeuchi, T. Tohyama, and S. Shin, *Nature Communications* **6**, 1 (2015).
 - ²⁰ M. Hashimoto, R.-H. He, K. Tanaka, J.-P. Testaud, W. Meevasana, R. G. Moore, D. Lu, H. Yao, Y. Yoshida, H. Eisaki, *et al.*, *Nature Physics* **6**, 414 (2010).
 - ²¹ K. Fujita, I. Grigorenko, J. Lee, W. Wang, J. X. Zhu, J. Davis, H. Eisaki, S.-i. Uchida, and A. V. Balatsky, *Physical Review B* **78**, 054510 (2008).
 - ²² Y. He, M. Hashimoto, D. Song, S.-D. Chen, J. He, I. Vishik, B. Moritz, D.-H. Lee, N. Nagaosa, J. Zaanen, *et al.*, *Science* **362**, 62 (2018).
 - ²³ X. Chen, M. Yu, K. Ruan, S. Li, Z. Gui, G. Zhang, and L. Cao, *Physical Review B* **58**, 14219 (1998).
 - ²⁴ S. Martin, A. Fiory, R. Fleming, L. Schneemeyer, and J. Waszczak, *Physical Review Letters* **60**, 2194 (1988).
 - ²⁵ Z. Li and *et al.*, in preparation.
 - ²⁶ Y. He, Y. Yin, M. Zech, A. Soumyanarayanan, M. M. Yee, T. Williams, M. Boyer, K. Chatterjee, W. Wise, I. Zeljkovic, *et al.*, *Science* **344**, 608 (2014).
 - ²⁷ M.-Y. Choi, W. E. Pickett, and K.-W. Lee, arXiv preprint arXiv:2005.03234 (2020).
 - ²⁸ S. Kivelson, *Physica B: Condensed Matter* **318**, 61 (2002).
 - ²⁹ C. Gros, B. Edegger, V. Muthukumar, and P. Anderson, *Proceedings of the National Academy of Sciences* **103**, 14298 (2006).
 - ³⁰ A. W. Sandvik, *Physical Review B* **57**, 10287 (1998).
 - ³¹ M. Norman, M. Randeria, H. Ding, and J. Campuzano, *Physical Review B* **57**, R11093 (1998).
 - ³² I. K. Drozdov, I. Pletikosić, C.-K. Kim, K. Fujita, G. Gu, J. S. Davis, P. Johnson, I. Božović, and T. Valla, *Nature Communications* **9**, 5210 (2018).
 - ³³ T. Devereaux and D. Einzel, *Physical Review B* **51**, 16336 (1995).
 - ³⁴ M. Hashimoto, E. A. Nowadnick, R.-H. He, I. M. Vishik, B. Moritz, Y. He, K. Tanaka, R. G. Moore, D. Lu, Y. Yoshida, *et al.*, *Nature Materials* **14**, 37 (2015).
 - ³⁵ C. Renner, B. Revaz, J.-Y. Genoud, K. Kadowaki, and Ø. Fischer, *Physical Review Letters* **80**, 149 (1998).
 - ³⁶ M. Hashimoto, I. M. Vishik, R.-H. He, T. P. Devereaux, and Z.-X. Shen, *Nature Physics* **10**, 483 (2014).
 - ³⁷ It should be noted that the Luttinger volume determined this way may also deviate from the actual filling in the presence of lingering correlation effects²⁹.
 - ³⁸ Without a superconducting gap, the van Hove point at $(\pi, 0)$ is only 7 meV below the Fermi energy. It is completely obscured in the superconducting state by the 16 meV gap.
 - ³⁹ Note that we do not intend this to be a realistic model for the cuprates. However, the question to address, namely, what impedes the superconducting phase coherence when the band structure contains flat band in part of the Brillouin zone, remains valid. Thus the simulation below aims to address a matter-of-principle question, rather than a quantitative description of the cuprate material.
 - ⁴⁰ The particle-hole asymmetry is due to the small momentum deviation from the exact \mathbf{k}_F in the finite lattice used for the simulation.